INTERNATIONAL JOURNAL OF OPTIMIZATION IN CIVIL ENGINEERING
Int. J. Optim. Civil Eng., 2022; 12(3):313-334

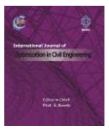

NUMERICAL AND EXPERIMENTAL INVESTIGATION OF WIND PRESSURE COEFFICIENTS ON SCALLOP DOME

F. Rezaeinamdar[1], M. Sefid[1*, †] and H. Nooshin[2]
[1]*Department of Mechanical Engineering, Yazd University, Yazd, Safaieh, Iran*
[2]*Department of Civil Engineering, University of Surrey, Guildford, Surrey GU2 7XH, UK*

ABSTRACT

The wind loads considerably influence lightweight spatial structures. An example of spatial structures is scallop domes that contain various configurations and forms and the wind impact on a scallop dome is more complex due to its additional curvature. In our work, the wind pressure coefficient (C_p) on the scallop dome surface is studied numerically and experimentally. Firstly, the programming language Formian-K is used for generating the scallop dome configuration. Then, the scallop dome scale model is designed using a CAD/CAM system, and it is constructed in fiberglass. Afterward, the wind tunnel of the atmospheric boundary layer is presented, and the scale model is applied for performing the tests so that the C_p is obtained. The scallop dome scale model was taken into account in numerical investigation. For simulation of the turbulent flow, Large Eddy Simulation (LES), Reynolds Stress Turbulence Model (RSM), the k-ε RNG, and k-omega Shear Stress Transport (k-ω SST) approaches were used. Lastly, we compared the wind pressure coefficients obtained by Computational Fluid Dynamics (CFD) with the results of the experimental investigation. As indicated by the results, the LES method, particularly, RSM model, can be applied because of lower computational costs for the analysis of other scallop dome configurations for obtaining C_p.

Keywords: wind pressure coefficient; CFD simulation; scallop dome; wind tunnel; experimental investigation; numerical investigation.

Received: 5 March 2022; Accepted: 9 April 2022

[*]Corresponding author: Department of Mechanical Engineering, Yazd University, Yazd, Iran
[†]E-mail address: mhsefid@yazd.ac.ir (M. Sefid)

1. INTRODUCTION

Spatial structures refer to structures that are used for covering buildings with large areas and covering surfaces with special architectural purposes. Thus, these structures allow construction of such places as meeting halls, large warehouses, sports stadiums, industrial halls, multipurpose exhibitions, churches, mosques, passenger terminals, and aircraft hangars.

Scallop domes refer to spherical domes with alternate grooves and ridges, which radiate from the dome center. The scallop domes as spatial structures present an attractive beautiful geometry, and thus, they are one of famous domes for buildings with large areas. Many examples of scallop domes can be mentioned worldwide as continuous or lattice shell domes. Some scallop domes built worldwide are indicated in Figs. 1-3. These types of domes are called 'scallop' because of the similarity of their shape to the marine shell. The term 'scalloping' means the process of turning a spherical dome to a scallop one. There are some parameters for defining scallop and other domes that have similar geometries. The definitions, back ground, tools, and terminology have been presented by Nooshin et al. (1997); Nooshin (2017) and Nooshin et al. (2017) for generating the configuration of scallop and similar domes. The wind loads considerably affect large lightweight structures, e.g., spatial structures. Since this type of structural form is light in comparison with building structures, wind loads are crucial, and seismic forces are of secondary importance. Since scallop domes contain various configurations and forms, the wind impact is complex. Scallop domes have higher stiffness compared to the correspondent spherical domes due to their additional curvature; However, the wind effect on a scallop dome is more complicated.

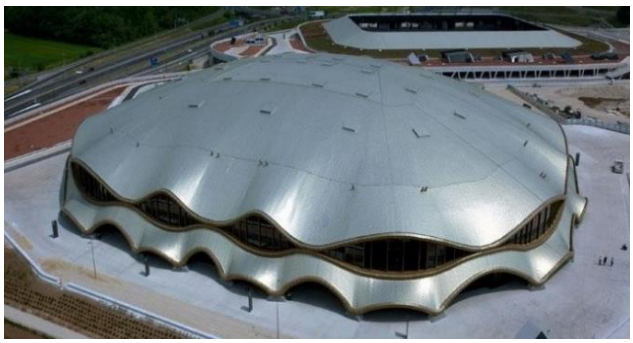

Figure 1. Multi-purpose sports hall (Slovenia)

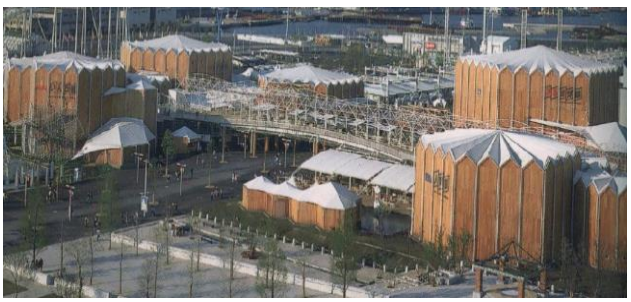

Figure 2. Yokohama Recreation Center (Japan)

Figure 3. Rungrado stadium (North Korea)

Various domes have been studied extensively and optimized by different metaheuristic optimization algorithms. Example can be found in Kaveh and Talatahari, (2011), Kaveh and Rezaei (2018), Kaveh and Javadi (2019), and Kaveh et al. (2021). Destruction and collapse of curve-shaped domes with strong winds have been reported in the past years. The structural failure induced by wind can be due to poor quality construction and/or insufficient wind-resistant design. Metro Stadium in the USA is indicated in Fig. 4that was damaged because of storm and wind load in 2010. Besides, Figs. 5 and 6 show the damage to the scalloped dome roof of St. Michael's Catholic Church in Biloxi (Mississippi) due to Hurricane Katrina in 2005.

Figure 4. Collapse of the American Metro Stadium resulting from storm and wind

Figure 5. Damage to the scalloped dome roof of St. Michael's church in Mississippi because of Hurricane Katrina

Figure 6. Damage to the scalloped dome roof of St. Michael's church in Mississippi because of Hurricane Katrina

There are a few studies on the scallop domes' behavior, the impact of geometric properties of scallop dome on its weight, and the earthquake effect, and just one work has numerically analyzed the wind flow effect on scallop domes with Parabolic grooves. The behavior of scallop domes and the impact of critical geometric properties of the scallop dome on its weight, the earthquake effect, and size optimization in scallop domes exposed to static loads were studied by Salajegheh and Kamyab (2011; 2013 and 2014). To this end, they used genetic and other algorithms. An efficient methodology was presented by Sheidaii (2013) and Babaei for designing large-scale scallop domes optimally with different dimensions and topologies in the plan using the genetic algorithm. Kamyab et al. (2013) studied the impact of arching styles on the scallop dome behaviors. As shown by their results, more efficient and lighter domes can be obtained by parabolic arching style with steep curve slopes compared to the sinusoidal arching style with smooth curve slopes.

Despite a large number of studies on CFD, a few works have investigated numerically the effect of wind on spherical domes and spatial structures with large roof. Baker (2007) and Blocken (2014) comprehensively reported the future, present, and past of wind engineering studies. Sarkar and Latchford (2000) studied the impact of fluctuating and mean wind loads on smooth and rough parabolic domes in simulated atmospheric boundary layer flow. Meroney et al. (2002) developed a numerical comparison and simulated the wind loads on

dual, rough, and flat domes immersing in a boundary layer. Horr et al. (2003) used CFD for presenting a formulation to generate a computational wind tunnel for deriving the pressure load on large-sized domes. Tamura et al. (2008) employed CFD methods, such as modified RANS and LES, to design wind-resistant buildings. Besides, they presented a guideline for the construction of a numerical model, which included choosing a turbulence model, computational domain size, needed numerical discretization, etc. Bahadori and Faghih (2009 and 2010) conducted a numerical and empirical study on the airflow effect over domed roof buildings for determining the distribution of air pressure over domed roofs using the k-ε RNG technique. The wind pressure on arched roofs was calculated by Kateris et al. (2012) by CFD, and they made a comparison with the Codes of Practice provisions. Ferreira and Vizotto (2015) conducted a numerical and empirical study on wind force impact on the hexagonal shells. Elkhoury (2016), evaluated the accuracy of the one-equation turbulence model in prediction of flows with massive separation in bluff bodies is evaluated against the k-ω-SST-Scale Adaptive Simulation (SAS) and the Spalart Allmaras (SA) models. Non-Linear Eddy-Viscosity closures around obstacles was used by Longo et al. (2017) and a new building influence area concept was proposed for presenting more reasonable alternatives to LES simulations without compensating for an acceptable level of accuracy. The wind flow effect on scallop domes with Parabolic grooves was studied by Sadeghi et al. (2017). Majdi et al. (2018) analyzed using CFD the interplay of a tornado wind on prism and dome structures. Elshaer et al. (2019) evaluated a four-story building with LES to examine the variation in the external and internal wind loads for various rates of supposed damages. Aly and Gol-Zaroudi (2020), using CFD and LES method, suggested new suggestions on the building model surrounded by mesh region size.

There are a few experimental investigations in the field of wind effect on spherical domes and spatial structures. The pressure field impacts on domes with varying span/rise ratios were investigated by Uematsu et al. (1997). An empirical investigation was conducted by Godoy and Portela (2005) to study the wind pressures and the behavior of steel tanks with dome and conical roofs. The effect of wind on a spatial lattice structure was studied by Li and Fu (2007) numerically and experimentally. The Reynolds number impact on the aerodynamic features of hemispherical domes was studied by Fu and Cheng (2010). Rizzo et al. (2011) and Rizzo (2012) examined the wind impact on the hyperbolic paraboloid roofs. The aerodynamics of the membrane structures was investigated by Michalski et al. (2011). Sun et al. (2013 and 2016) analyzed the effect of wind tunnel experiments on different rise-to-span spherical domes and a model was presented for the domes' wind pressure spectra. The wind loading on cylindrical roofs was modelled by Qui et al. (2014), given the Reynolds number effect in a low turbulence uniform flow. The impact of bumps in altering the wind pressure on buildings was experimentally studied by Chevula et al.

Because of the grooves and ridges and geometrical shape of the scallop domes, the wind effects on the scallop domes are more critical and more complicated than other domes, most of which have uniform levels. The current study investigates the wind pressure coefficients on the scallop domes. The C_p is defined as a dimensionless number describing the relative pressures through a flow field in fluid dynamics. At a point near the body, the pressure coefficient is independent of the body size, which is specified at critical locations surrounding the model. It is possible to use the pressure coefficients for predicting the fluid pressure in the

critical areas surrounding a full-size spatial structure.

It is challenging to obtain pressure coefficient when the dome has an unconventional and more complicated geometry and when it is possible to directly cover it by the standard tables of conventional geometric shapes. Because of the lack of pressure coefficients for complex structures, like the scallop domes, for which there is no experimental research, the wind pressure distribution on these structures is specified by scale models 'experiments in a wind tunnel and computational simulations.

In the present paper, we investigated one of the selected forms of scallop dome in the wind tunnel. In the following, different models of numerical analysis are used and the experimental research results are compared. Then, we introduce the numerical approach with the most optimal error and computational cost.

2. WIND TUNNEL TESTS OF THE SCALLOP DOME

Using the pressure measurements on scale models with the appropriate accuracy, the wind effects on actual domes can be determined. The dome's aerodynamic behavior, the 3D forms of the domes, the Reynolds number, and the average profile of the wind velocity (the spectral distribution and intensity) are the significant factors for these tests. Using the Reynolds number, we can check the similarity between the actual domes and the scale models. Reynolds number indicates the ratio between viscous forces and inertia, which is a dimensionless parameter. If there is a dynamic similarity between the two systems, the pressure distributions and flow patterns are similar between the actual domes and the scale models.

2.1 Wind tunnel of the atmospheric boundary layer

For obtaining pressure coefficients, we built a scallop dome scale model, and it was instrumented for the wind tunnel tests of atmospheric boundary layer of the School of Mechanical Engineering at Kerman Islamic Azad University (Fig. 7). The wind tunnel of the atmospheric boundary layer is described as a linear open-circuit tunnel that has a reversed axial fan causing suction of air. The height, length, and width of the tunnel are 2.5, 13.5 and 3.5 m, and the section has 1.8 m length. The cross-section has 0.75m width and 0.75m height (cross-sectional area as $0.56m^2$). In the test section, the highest velocity is 30 m/s (km/h 108). Variation of the air speed with continuity from 3 to 30 m/s is performed through the fan rotation speed variation by 1% controller Accuracy. For reduction of the large vortices and simulation of the laminar flow, through the inlet nozzle, the air enters and passes the Honey comb nylon screen. The cross section is decreased after the screen. Thus, the flow becomes laminar, and the turbulence is eliminated. After air passes through the test section and scale model, it leaves through the tunnel diffuser.

Figure 7. Schematic view of open-circuit wind tunnel

2.2 Wind tunnel tests of the scallop dome

For constructing the scallop dome model, firstly, we should determine the dome's configuration and geometry based on the scallop generation rules.

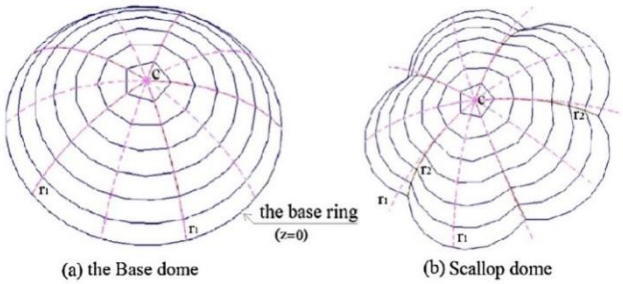

Figure 8. The circumscribing spherical dome (a), A scallop dome (b)

There are two meridional ribs (r_2) and (r_1) in scallop dome illustrated in Fig. 8(b), dividing the spherical dome into equal sectors. The base dome is defined by arch $r_1$defines and the grooved arch is determined by arch r_2 defines the grooved arch. The vertical and/or horizontal distortion can happen. With the vertical curving, the dome's circular plan is maintained, while the horizontal curving makes segments as convex. The arch distortion might follow sinusoidal or parabolic law in a negative or positive direction. In our work, the effect of wind on the scallop dome is considered with six identical arched segments. In this investigation, the dome segments are arched by sinusoidal law and the aspect ratio k = H/D is 0.5, where H denotes the dome rise, and D represents the diameter. The prominence of the ring is defined as the horizontal move of a mid-segmental point of a circumferential ring. The furthest ring from the crown presents the greatest prominence, which is known as the prominence of the dome. The prominence of the dome is negative 0.1 in the present work, and the maximum vertical movements of components occurring at the middle of the arches are the amplitude considered 0 in our work.

The overall size of the wind tunnel test section influences geometric scale. The range of typically used scales is between 1:300-1:600 for large structures and down to 1:100 or less for smaller buildings, which only surface layer simulation is required for them. A 1/100 scale

model was developed in the present work, with a dome rise of 14.5 cm and a diameter of 29 cm. We selected this scale given the accuracy expected from the measurements and the wind tunnel test section size. The test section allows conducting test on models with small sizes, without edge effects. Using models with the largest dimension is essential in wind tunnel tests with small cross-sections. Thus, the model's maximum frontal area must be 5-10 percent of the inlet cross-section of the wind tunnel. That is, generally, the tunnel cross-section blockage is retained under 10 percent (Barlow et al. 1999). Block coefficient, i.e., the ratio between the inlet cross-sectional area of the wind tunnel (0.75×0.75 m) and the frontal section of the scallop dome model (0.0353 m^2), was 6.3 percent in the present work.

A scallop shell was developed (Fig. 10) after configuring the scallop dome and generating a 1/100 scale model using Formian-K software (Nooshin et al. 2016) (Fig. 9).

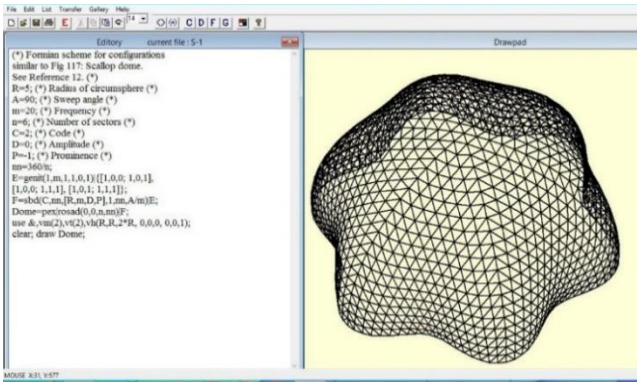

Figure 9. Configuration of the scallop dome using Formian-K

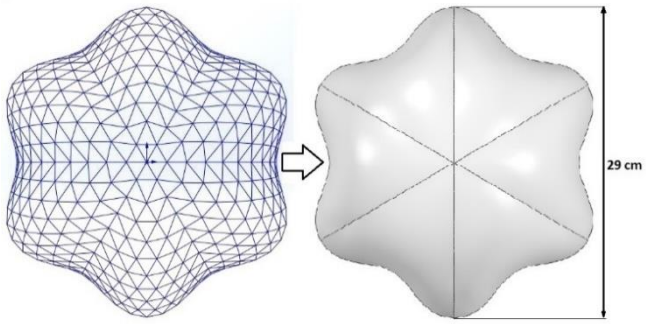

Figure 10. Generation of the shell for the scallop dome

Within three steps, we built the scallop scale model. Firstly, the mold was made in Beech wood. In the second step, a 3D-CNC router was developed using a CAD/CAM system, lathing the scale scallop dome shape (Fig. 11).

Figure 11. Block in wood at CNC machine for generating
A scallop dome formwork

Lastly, wooden formwork was used to build scallop dome model by applying fiberglass layers with a thickness of 3 mm. The painting was used for the removal of any imperfection (Fig. 12).

Figure 12. Scallop dome model in fiberglass

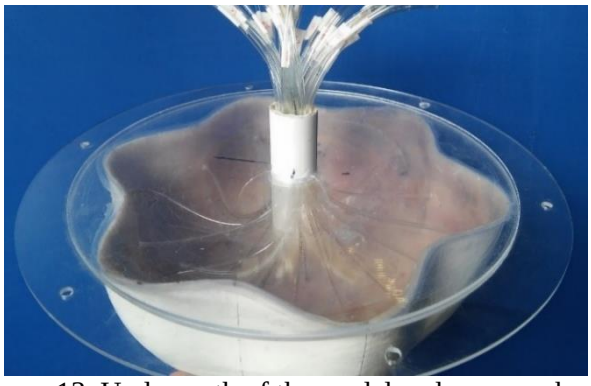

Figure 13. Underneath of the model and pressure hoses

A system integrated with pressure hoses and sensors and a computer was used for instrumenting the scallop fiberglass model (Fig.13). At five levels, pressure measuring hoses were located on the top of the arch and the depth of groove of the scallop dome: 3.6, 7.4, 11.1, 14, and 14.5 cm from the surface of the test section. The measuring hose was placed only at one point at the level of 14.5 cm at the top of the dome (Fig. 14). Using an additional sensor, the free-stream pressure was measured in the tunnel through the Pitot tube (Fig. 15). Negligible deformations are assumed dome surface and structure in this paper.

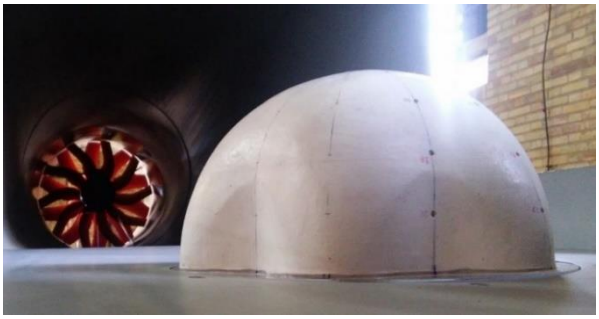

Figure 14. Scale model of scallop dome in fiberglass at the wind tunnel

Figure 15. A view of the model under test in the wind tunnel

The velocity profile occurring in the atmosphere should be simulated in the wind tunnel according to roughness or the location of the building. Eq. (1) can be used for expressing the boundary layer's wind velocity profile for various types of roughness and near the ground used in the test:

$$\frac{V_h}{V_H} = \left(\frac{h}{H}\right)^{a} \tag{1}$$

where V_H denotes the average wind velocity at the gradient height of H, V_h is represents the average wind velocity at elevation h, the , and exponent “a” denotes a constant. a = 0.28 and H = 400m are recommended for small cities (Barlow et al.1999). Therefore, Eq. (2) givens the desired wind velocity profile:

$$\frac{V_h}{V_{400}} = \left(\frac{h}{400}\right)^{0.28} \quad (2)$$

V_{400}=48.6 m/s was considered in this simulation (Faghih and Bahadori 2009). Urban and suburban boundary layers modeling at the wind tunnel needs elements to generate turbulence and wind velocity profile (Ghazal et al. 2020). For modification of the atmospheric boundary layer in test section for producing and simulating the desired wind velocity profile, we placed steel bars with a diameter of 5 mm across the beginning of the wind tunnel test section at different spacing. An acceptable wind velocity profile was obtained by altering the spacing between the steel bars (11 times) and through a trial and error process (Faghih and Bahadori 2009). The final steel bars spacing and the obtained wind velocity profile downstream of the steel bars and upstream of the scallop model are shown in Figs. 16 and 17.

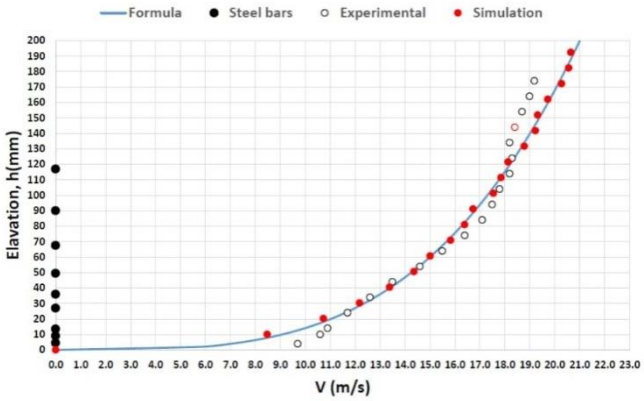

Figure 16. The steel bars used at the beginning of wind tunnel test section (left), the wind velocity profile created in the wind tunnel (right)

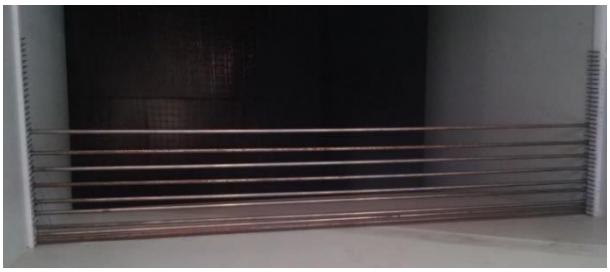

Figure 17. The steel bars used at the beginning of wind tunnel test section

Considering Eq. 2, the airflow velocity on the top part of the scallop dome (14.5m) is 19.19 m/s.

After conducting the test, we obtained the pressure from measurements. Eq. (3) was used for determining the wind C_p at different points on the scallop dome:

$$C_p = \frac{2\,(P - P_\infty)}{\rho\, V^2} \quad (3)$$

where P-P∞ denotes pressure difference between free-stream pressure P_∞ and dome surface pressure P, V indicates air velocity, and ρ represents the density. In this relation, velocity was 19.19 m/s that was calculated from the top of the scallop dome model at 145 mm. The wind tunnel test results are represented in Figs. 22–26, and black spots indicate the values of changes in pressure coefficient in the interval of [0,180] degrees dome surface at heights of 36, 74, 111, 140 and 145 mm.

3. COMPUTATIONAL FLUID DYNAMICS (CFD) MODEL OF THE SCALLOP DOME

The CFD model of the scallop dome was simulated in the identical wind flow situations in the wind tunnel for obtaining the wind pressure coefficients over the scale scallop model. Considering the numerical simulation of the wind flow near bluff bodies, for example, civil structures separating flow over an essential part of its surface because of its shape, it is possible to conduct CFD at large Reynolds numbers either through high-fidelity simulations, like Large Eddy Simulation (LES) or low-fidelit simulations, like Reynolds-averaged Navier-Stokes (RANS) (Peric and Ferziger 2012). We used commercial software, as well as the k-epsilon RNG (k-ε RNG), Reynolds Stress Turbulence Model (RSM), and k-omega Shear Stress Transport (k-ω SST) as RANS models, and LES technique to simulate the turbulent flow.

Fig. 18 indicates the solution domain's dimension and the boundary conditions. Given the scallop dome's location and design in the wind tunnel and considering the circumstances of the computational range, and also for reducing the computational cost, we used symmetry and half of the model for simulation purposes. Boundary conditions of the wind tunnel's roof, ground, and wall were regarded as Wall and Outlet boundary conditions as Pressure outlet.

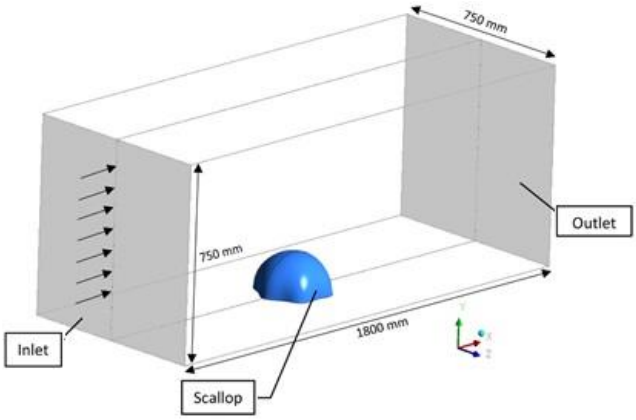

Figure 18. The dimensions and boundary conditions of the solution space

Eq. (2) was used for simulation of a near-ground wind velocity profile for the height variation for the inlet surface, using User Defined Functions (UDF) (Fig. 16).

The software mesh discretization is subject to the characteristics of the tunnel wind, including the wind velocity (v = 20 m/s), height (b = 0.75 m), the width (a = 0.75 m) of the

wind tunnel cross-section, and the kinematic viscosity ($\mu = 0.0000156\ m/s^2$). Using equations (4)-(7), the Reynolds number (Re), the height of first boundary layer (L_y), the hydraulic diameter (D_H), and the height of the boundary layer (C_l) are calculated.

Eq. (4) can be used for defining the hydraulic diameterD_H,for rectangular cross-section areas with height (b) and width (a) in internal flow situations:

$$D_H = \frac{4ab}{(2a + 2b)} \tag{4}$$

The Reynolds number (Re) is obtained by Eq. (5) using the kinematic viscosity (μ), the hydraulic diameterD_H, and the wind velocity (v)as follows:

$$Re = \frac{v.D_H}{\mu} \tag{5}$$

Using Eq. (6), we define the height of the boundary layer C_l:

$$C_l = \frac{0.035\ D_H}{Re^{(\frac{1}{7})}} \tag{6}$$

Using Eq. (7), the height of the first layer L_y of the boundary layeris obtained:

$$L_y = \frac{\sqrt{74} * D_H}{Re^{(\frac{13}{14})}} \tag{7}$$

The parameters calculated from Equations (4) -(7) are presented in Table 1.

Table 1: CFD model parameters

Setup mesh parameters	
First layer height (L_y)	0.00001865 m
Hydraulic diameter (D_H)	0.75 m
Boundary layer thickness (C_l)	0.00368964
Reynolds number (Re)	922596

The geometric structure of the scallop dome was examined, and given the significance of employing a regular grid in reduction of computational costs and increasing the calculation accuracy, we used a poly-hex core composite grid considering parameters of table 1. The mesh details of the test section of the wind tunnel are presented in Fig. 19. Smaller elements are provided by the mesh discretization in the subdomain where the boundary layer change happens. It is also because of the presence of pressure and velocity gradients.

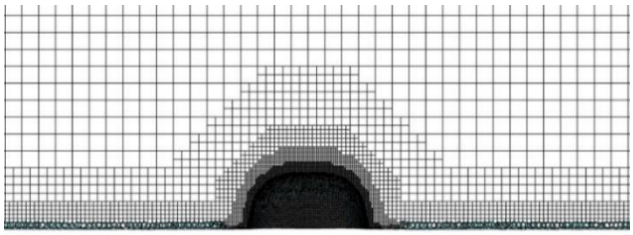

Figure 19. Mesh of wind tunnel test section from the front view

The number of meshes in the computational are a considerably influences the numerical solution results. When the number of meshes is increased, and with focusing on high gradient areas, computational accuracy is also increased. Besides, computational mesh elements cannot be fragmentized and fine-tuned to infinity. Hence, the optimal mesh can be achieved by investigating the meshes. In the present study, RSM model was used for investigating mesh dependency. The pressure coefficient on the scallop dome surface is the criterion for the solution independence from the number of meshes. Moreover, experimental data validated the accuracy of the simulated graph of pressure coefficient changes. Changes in pressure coefficients were investigated in the range of [0, 180] degrees, in the number of meshes 253005, 356505, 466268, 643093, and 820830 at heights of 36, 74, 111, 140, and 145 mm. Fig. 20 indicates C_p diagram at a height of 36 mm. The graph represented in this figure examines the impact of number and size of the mesh on the CFD results accuracy. According to these results, with increasing the number of mesh, the result accuracy increased, approximating more to the experimental results. The size of the mesh does not cause a serious change in the C_p below a certain range, and increasing number of mesh from 643093 to 820830 does not significantly affect the C_p results. Consequently, given subtle changes in pressure coefficient and the computational cost, the mesh number 643093 was chosen for subsequent studies.

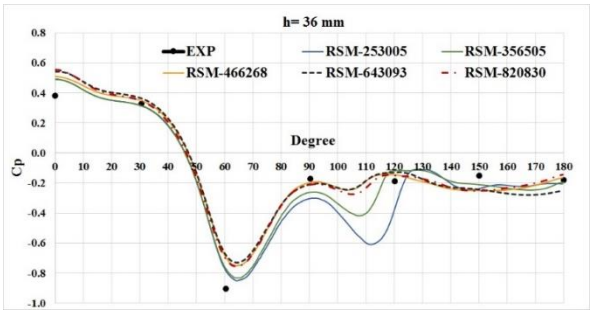

Figure 20. The impact of number and size of the mesh over the C_p accuracy in the range of [0, 180] at 36 mm height

LES is one of the methods for simulation that was examined in the present paper. Since this model is time-dependent, we studied the time steps for this model for pressure coefficients in time steps of 1, 0.5, 0.1, 0.05, 0.01, 0.005 s, with a total time of 5 s, in the range of [0, 180] degrees at heights of 36, 74, 111, 140, and 145 mm on the dome surface. Fig. 21 indicates the

results of $C_p$results are shown in for the 36 mm height. As shown by the studies, the time steps of 0.01 and 0.005 s showed a good match. The time step of 0.01 s was selected for the LES model for reducing the computational cost resulting from the very small differences in the results.

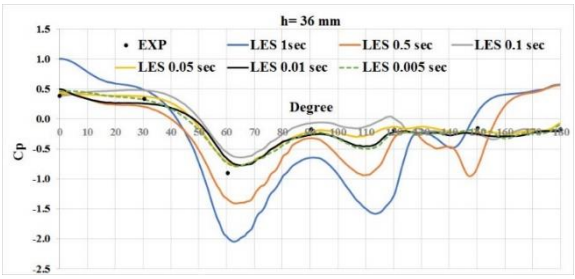

Figure 21. The results of C_p for LES model in 6 time steps in the range of [0, 180] and the 36 mm height

4. COMPARING EMPIRICAL AND NUMERICAL RESULTS OF WIND PRESSURE COEFFICIENTS ON SCALLOP DOME

Following conducting time step studies in LES method, turbulence models, including k-ω SST, k-ε RNG, LES and RSM method with the number of mesh 643093 were used for simulating the scallop dome. Pressure coefficient changes at heights of 36, 74, 111, 140, and 145 mm of the dome surface in the range of [0, 180] degrees are compared in Figs. 22 to 26. The vertical axes in the diagrams represent the C_p, where the negative numbers represent wind suction and the positive ones represent wind pressure. The circumferential angle denotes the variable of the horizontal axis of the graphs, which varies in the [0, ±180] interval. However, because of the dome's plan symmetry, the figures show only the results for the positive angle values. These graphs show that a groove results in an indentation in the C_p graph. We compared the results of the pressure coefficients on the scallop model achieved by the software for simulating the CFD with the wind tunnel test results for the scallop dome with the identical wind flow conditions (Figs. 22–26). Similar front pressure distributions to the wind tunnel data were predicted by all numerical models, as expected.

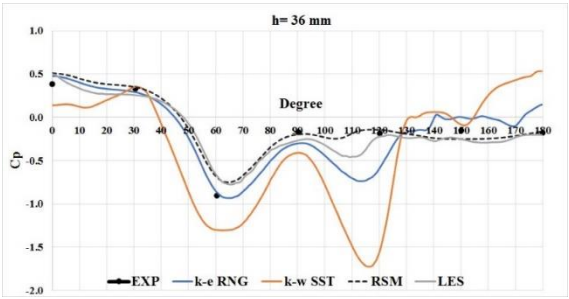

Fig. 22 Comparison of numerical and empirical results of $C_p$in the range of [0, 180] at the 36mm height

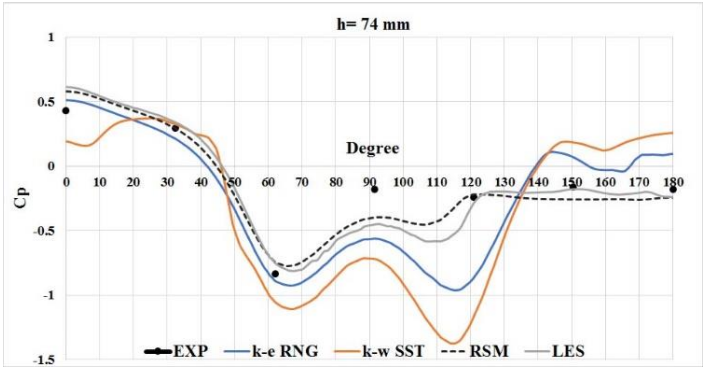

Figure 23. Comparison of numerical and empirical results C_p in the range of [0, 180] at the 74mm height

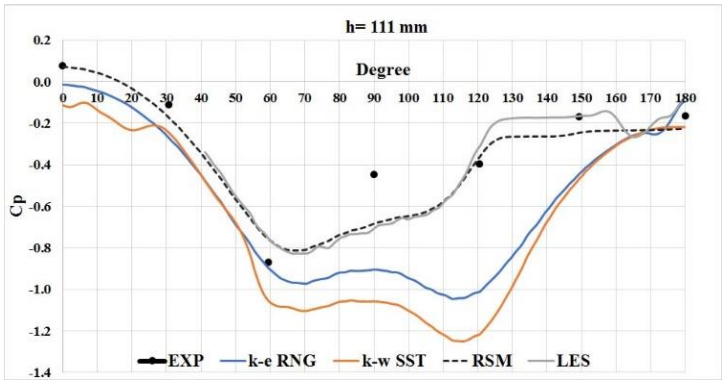

Figure 24. Comparison of numerical and empirical results of C_p in the range of [0, 180] at the 111mm height

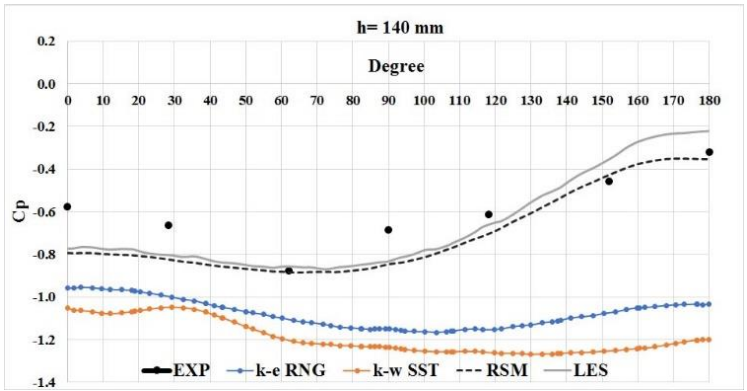

Figure 25. Comparison of numerical and empirical results of C_p in the range of [0, 180] at the140mm height

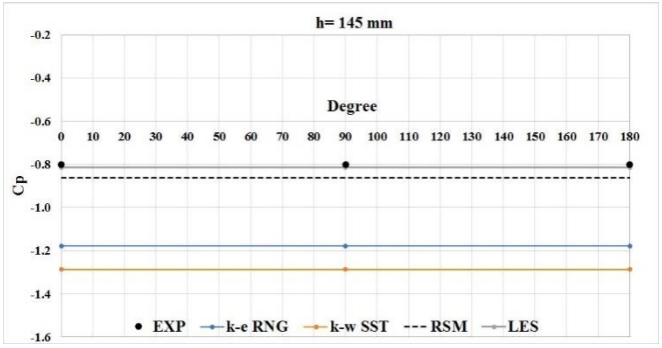

Figure 26. Comparison of numerical and empirical results of C_p in the range of [0, 180] at the145mm height

The contour areas of C_p indicate the wind pressure coefficients in the scallop dome surface (Figs. 28, 29). Table 2 presents the results of Figs. 22-26 and the time of calculations obtained from the software. It presents a qualitative and quantitative comparison of the employed models in terms of the accuracy of the simulation results and the calculation costs.

Table 2: Qualitative (accuracy) and quantitative (computational cost) comparison of the used models

Model	Computational costs (Second)	Accuracy of Calculations	Conclusions
k-ε RNG	322	low	unacceptable
k-ω SST	162	low	unacceptable
RSM	871	Good	acceptable
LES	5502	Good	Conditional acceptance

As illustrated by Figs. 22–26, LES provides the appropriate distribution of pressure on the scallop dome surface. The RANS models used in this work provided a correct prediction of the front pressure distribution. However, the RANS models, except RSM, showed unsatisfactory performance regarding the reattachment points on the side and top surfaces.

The isometric view of the pressure coefficient changes on the dome surface and the velocity-based flow lines in the computational simulation software near the dome is shown in Fig. 27. as a result of the protrusions and the scallop dome protrusions, the wind flow causes turbulent flow vortices in the back of the dome and the separation of the flow, leading to changes in pressure on the respective surfaces.

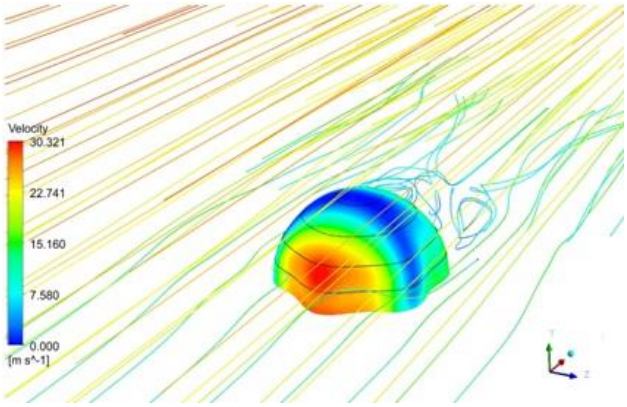

Figure 27. Isometric view of contour changes in pressure coefficient on scallop dome and flow lines based on velocity

As a result of the creation of a high-pressure area on the windward side, the air around the sides and up over the top of the scallop dome is pushed. A part of the air flows descending, and an eddy is created around the model at the downwind. A considerable turbulent flow is created in this area. Consequently, uncertainty and a difference can be expected between the numerical and experimental values of C_p obtained for this area.

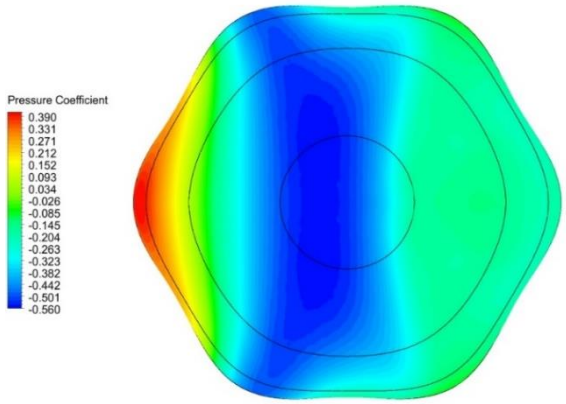

Figure 28. The contour areas of C_p all over the scallop dome surface

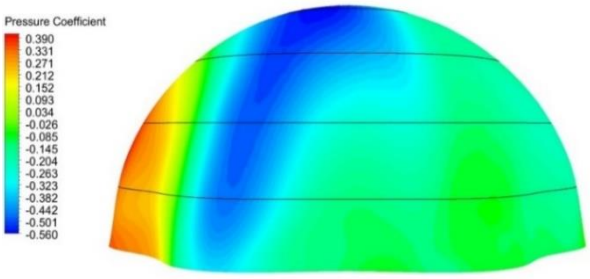

Figure 29. The contour areas of C_p all over the scallop dome surface

5. CONCLUSIONS

When the building geometry is not included in the conventional geometrical shapes tabulated by the different stands and codes, it is a challenging task to accurately determine the pressure coefficients. Since there are many configurations and forms in scallop domes, the effect of wind is complicated. In this case, wind tunnel tests are generally used that provide accurate pressure coefficients. However, numerical simulation and CFD are commonly employed since wind tunnel tests are costly and time-consuming.

An accurate time-dependent analysis, e.g., LES, is needed for using CFD for wind load estimation since it allows predicting peak-type of quantities, like the maximum response of a structure or a peak pressure. We compared the results obtained from CFD with the corresponding wind tunnel empirical data and it was shown that both the RANS models and LES method could reasonably predict the front pressure coefficients in the range of [0, ±90]. The main difference between the numerical and empirical results was behind the model because of a separation. The LES model captured flow on the side and top of the scallop dome, particularly in the range of [90, ±180], as well as bottom of grooves and top of arches, while the performance of RANS models, except RSM was not satisfactory for the reattachment point on the side and top surfaces. LES, however, presented a better overall consistency with the experimental data compared to RANS, though with a longer computation time. In this work, the computational cost related to LES was approximately seven times higher than the RSM, as a RANS model.

As demonstrated by the results, the RSM model and LES method can be used for future applications for analyzing other scallop dome configurations for obtaining C_p. However, the RSM model is more preferred because of lower computational costs.

Acknowledgements: All wind tunnel experiments were conducted in the Department of mechanical engineering, Islamic Azad University, Kerman Branch. The authors appreciate A. Saeidinezhad and A. Namjoo for valuable help in the wind tunnel experiments.

REFERENCES

1. Babaei M, Sheidaii M. Optimal design of double layer scallop domes using genetic algorithm, *J Appl Math Mech* 2013; **37**(4): 2127-2138. https://doi.org/10.1016/j.apm.2012.04.053.
2. Baker CJ. The past, present and future of wind engineering, *J Wind Eng Ind Aerod* 2007; **95**: 843[70.
3. Blocken B. 50 years of computational wind engineering: past, present and future, *J Wind Eng Ind Aerod* 2014; **129**: 69–102.
4. Cheng CM, Fu CL. Characteristic of wind loads on a hemispherical dome in smooth flow and turbulent boundary layer flow, *J Wind Eng Ind Aerod* 2010; **98**: 328-44.
5. Chevula S, Sanz-Andres A, Franchini S. Aerodynamic external pressure loads on a semi-circular bluff body under wind gusts, *J Fluids Struct* 2015; **54**: 947–57. https://doi.org/10.1016/j.jfluidstructs.2015.02.004.

6. Elkhoury M. Assessment of turbulence models for the simulation of turbulent flows past bluff bodies, *J Wind Eng Ind Aerod* 2016; **154**: 10-20. https://doi.org/10.1016/j.jweia.2016.03.011.
7. Elshaer A, Bitsuamlak G, Bdallah H. Variation in wind load and flow of a low-rise building during progressive damage scenario, *Wind Struct* 2019; **28**(6): 389-404. https://doi.org/10.12989/was.2019.28.6.389.
8. Faghih AK, Bahadori MN. Experimental investigation of air flow over domed roofs, *Iran J SCI Technol B* 2009; **33**(B3): 207-16.
9. Faghih AK, Bahadori MN. Three-dimensional numerical investigation of air flow over domed roofs, *J Wind Eng Ind Aerod* 2010; **98**(3): 161–8. https://doi.org/10.1016/j.jweia.2009.10.012.
10. Fu JY, Li QS. Wind effect on the world's longest spatial lattice structures loading characteristics and numerical prediction, *J Constr Steel Res* 2007; **63**(10): 1341–50. https://doi.org/10.1016/j.jcsr.2006.12.001
11. Ghazal T, Chen J, Aboutabikh M, Aboshosha H, Elgamal S. Flow-conditioning of a subsonic wind tunnel to model boundary layer flows, *Wind Struct* 2020; **30**(4): 339-66. https://doi.org/10.12989/was.2020.30.4.339.
12. Horr AM, Safi M, Alavinasab SA. Computational wind tunnel analyses for large domes using CFD theory, *Int J Space Struct* 2003; **18**(2): 85-104. https://doi.org/10.1260/026635103769518206.
13. Kamyab R, Salajegheh E. Prediction of nonlinear time history deflection of scallop domes by neural networks, *Int J Optim Civil Eng* 2011; **1**(3): 419-32. http://ijoce.iust.ac.ir/article-1-48-en.html.
14. Kamyab R, Salajegheh E. Size optimization of nonlinear scallop domes by an enhanced particle swarm algorithm, *Int J Civil Eng* 2013; **11**(2): 77-89. http://ijce.iust.ac.ir/article-1-731-en.html.
15. Kamyab R, Salajegheh E. Optimum design of scallop domes for dynamic time history loading by harmony search-firefly algorithm, *Int J Optim Civil Eng* 2014; **4**(2): 273-91. http://ijoce.iust.ac.ir/article-1-174-en.html.
16. Kateris DL, Fragos VP, Kotsopoulos TA, Martzopoulou AG, Moshou D. Calculated external pressure coefficient on livestock buildings and comparison with Euro code 1, *Wind Struct* 2012; **15**(6): 481–94. https://doi.org/10.12989/was.2012.15.6.481.
17. Kaveh A, Talatahari S. Geometry and topology optimization of geodesic domes using charged system search, *Struct Multidis Optim* 2012; **43**(2): 215-29.
18. Kaveh A, Rezaei M. Optimal design of double layer domes considering different mechanical systems via ECBO, *Iranian J Sci Technol* 2012; **42**(4) 333–44.
19. Kaveh A, Javadi SM. Chaos-based firefly algorithms for optimization of cyclically large-size braced steel domes with multiple frequency constraints, *Comput Struct* 2012; published online, **214**(2019): 28-39. https://doi.org/10.1016/j.compstruc.2019.01.006.
20. Kaveh A, Amirsoleimani P, Dadras Eslamlou A, Rahmani P. Frequency-constrained optimization of large-scale dome-shaped trusses using chaotic water strider algorithm, *Struct* 2021.
21. Letchford CW, Sarkar PP. Mean and fluctuating wind loads on rough and smooth parabolic domes, *J Wind Eng Ind Aerod* 2000; **88**(1): 101-17.

https://doi.org/10.1016/S0167-6105(00)00030-1.
22. Longoa R, Ferrarottia M, García Sánchezb C, Derudie M, Parentea A. Advanced turbulence models and boundary conditions for flows around different configurations of ground-mounted buildings, *J Wind Eng Ind Aerod* 2017; **167**: 160-82. https://doi.org/10.1016/j.jweia.2017.04.015.
23. Majdi AA, Selvam Y, Panneer R, Prakash J. A comparison of the forces on dome and prism for straight and tornadic wind using CFD model, *Wind Struct* 2018; **26**(6): 369-82. https://doi.org/10.12989/was.2018.26.6.369.
24. Meroney RN, Letchford CW, Sarkar PP. Comparison of numerical and wind tunnel simulation of wind loads on smooth, rough and dual domes immersed in a boundary layer, *Wind Struct* 2002; **5**(2): 347-58. https://doi.org/10.12989/was.2002.5.2_3_4.347.
25. Michalski A, Kermel PD, Haug E, Ohner RL, Uchner RW, Bletzinger K. Validation of the computational fluid-structure interaction simulation at real-scale tests of a flexible 29 m umbrella in natural wind flow, *J Wind Eng Ind Aerod* 2011; **99**(4): 400–13. https://doi.org/10.1016/j.jweia.2010.12.010.
26. Mousaad Aly A, Gol-Zaroudi H. Peak pressures on low rise buildings: CFD with LES versus full scale and wind tunnel measurements, *Wind Struct* 2020; **30**(1): 99-117. https://doi.org/10.12989/was.2020.30.1.099.
27. Nooshin H. Formex configuration processing: a young branch of knowledge, *Int J Space Struct* 2017; **32**: 136-48.
28. Nooshin H, Kamyab R, Samavati OA. Exploring scallop forms, *Int J Space Struct* 2017; **32**: 84-111. https://doi.org/10.1177/0266351117736968.
29. Portela G, Godoy LA. Wind pressures and buckling of cylindrical steel tanks with a dome roof, *J Constr Steel Res* 2005; **61**(6): 808–24. https://doi.org/10.1016/j.jcsr.2004.11.001.
30. Qiu Y, Sun Y, Wu Y, Tamura Y. Modelling the mean wind loads on cylindrical roofs with consideration of the Reynolds number effect in uniform flow with low turbulence, *J Wind Eng Ind Aerod* 2014; **129**: 11–21. https://doi.org/10.1016/j.jweia.2014.02.011.
31. Rizzo FD, Asidia P, Lazzari M, Procino L. Wind action evaluation on tension roofs of hyperbolic paraboloid shape, *Eng Struct* 2011; **33**(2): 445–61. https://doi.org/10.1016/j.engstruct.2010.11.001.
32. Rizzo F. Wind tunnel tests on hyperbolic paraboloid roofs with elliptical plane shapes, *Eng. Struct* 2012; **45**: 536–58. https://doi.org/10.1016/j.engstruct.2012.06.049.
33. Sadeghi H, Heristchian M, Aziminejad A, Nooshin H. Wind effect on grooved and scallop domes, *Eng Struct* 2017; **148**: 436-50. https://doi.org/10.1016/j.engstruct.2017.07.003.
34. Sun Y, Qiu Y, Wu Y. Modelling of wind pressure spectra on spherical domes, *Int J Space Struct* 2013; **28**(2): 87–100. https://doi.org/10.1260/0266-3511.28.2.87.
35. Tamura T, Nozawa K, Kondo K. AIJ guide for numerical prediction of wind loads on buildings, *J Wind Eng Ind Aerod* 2008; **96**(10-11): 1974-84. https://doi.org/10.1016/j.jweia.2008.02.020.
36. Uematsu Y, Yamada M, Inoue A, Hongo T. Wind loads and wind-induced dynamic behavior of a single-layer latticed dome, *J Wind Eng Ind Aerod* 1997; **66**(3): 227–48. https://doi.org/10.1016/S0167-6105(97)00133-5.

37. Vizotto I, Ferreira AM. Wind force coefficient on hexagonal free form shells, *Eng. Struct* 2015; **83**: 17–29. https://doi.org/10.1016/j.engstruct.2014.10.038.
38. Barlow JB, Rae WH, Pope A. *Low-Speed Wind Tunnel Testing*, (3rd Edition), John Wiley & Sons, New York, USA, 1999.
39. Ferziger JH, Peric M. *Computational Methods for Fluid Dynamics*, Springer, Springer, Berlin, Heidelberg, Germany, 2012.
40. Kamyab R, Nooshin H, Salajegheh E. The effect of arching styles on the behavior of scallop domes, *Fourth National Conference on Earthquake and Structural*, Kerman, Iran, April, 2013.
41. Nooshin H, Tomatsuri H, Fujimoto M. Scallop Domes, *IASS97. Symposium on Shell & Spatial Structures: Design, Performance & Economics*, Singapore, 1997.
42. Sun Y, Su N, Wu Y, Shen S. Equivalent static wind load for large span spherical domes, *Proceedings of the IASS Annual Symposia, IASS Tokyo Symposium: Spatial Structures in the 21st Century – Extreme Loads & Disasters*, pp: 1-8(8)
43. Nooshin H, Sabzali A, Samavati OA. Basics of Formian-K, 2016, http://www.formexia.com/.